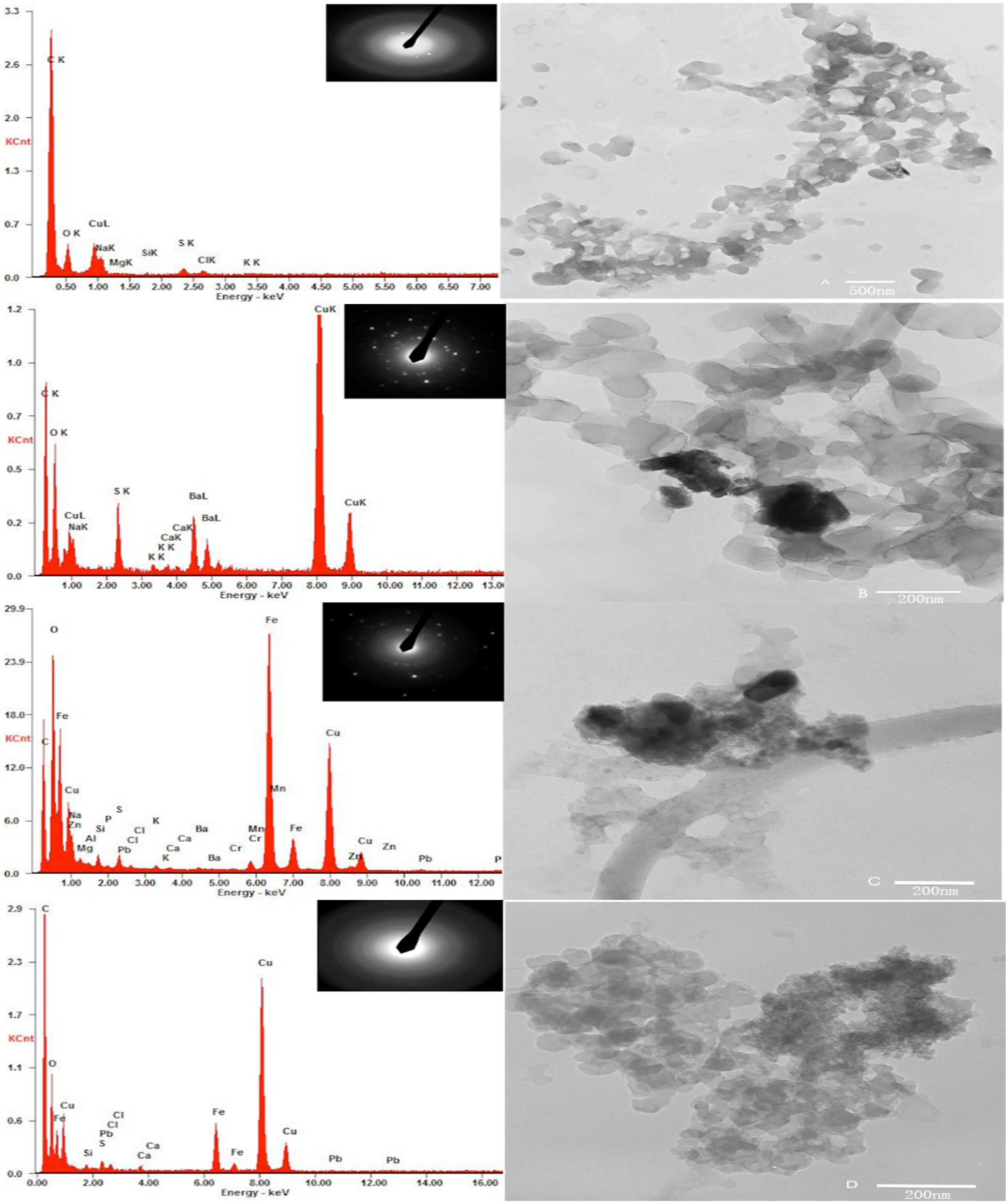

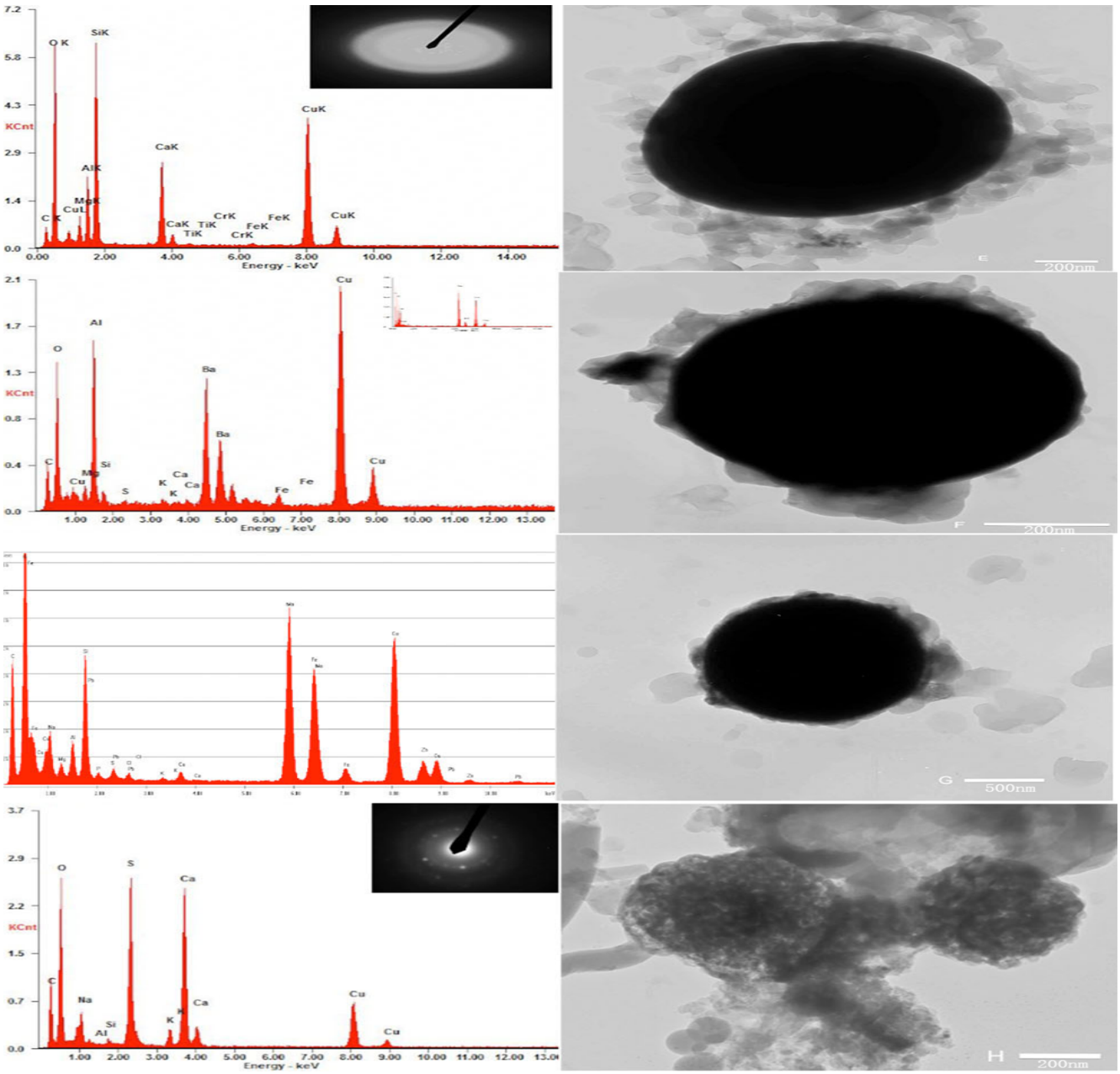

Figure S1 High-resolution microstructure of electron microscope images (right, white line is a standard index) and EDX spectra showing particle chemistry (left, in the inset electron diffraction pattern (EDP)) of $PM_{2.5}$ samples: A. airborne organic substance (length 500 nm), such as a typical element carbon aggregate emitted from a high-temperature combustion system (Lack et al., 2014), where the diffuse diffraction rings in the EDP prove that the material is truly amorphous; B. airborne organic substance with absorbed mineral particles (length 200 nm), shown as crystallite gypsum; C. airborne organic substance with absorbed mineral particles (length 200 nm), shown as microcrystallite siderite containing Mn, Pb, etc.; D. airborne organic substance with absorbed trace traces (length 200 nm), containing Fe, S, Pb, Cl, etc.; E. airborne organic substance with absorbed spherulitic microbeads (length 200 nm), shown as the amorphous silicate; F. airborne organic substance with absorbed spherulitic microbeads (length 200 nm), shown as barium aluminate mineral with an inset showing trace siderite peaks; G. airborne organic substance with absorbed trace metals (length 500 nm), EDX shown as Mn-Fe-Zn-Pb; and H. airborne organic substance associated with mineral particles (length 200 nm), shown as authigenic (secondary genic) microcrystallite gypsum.

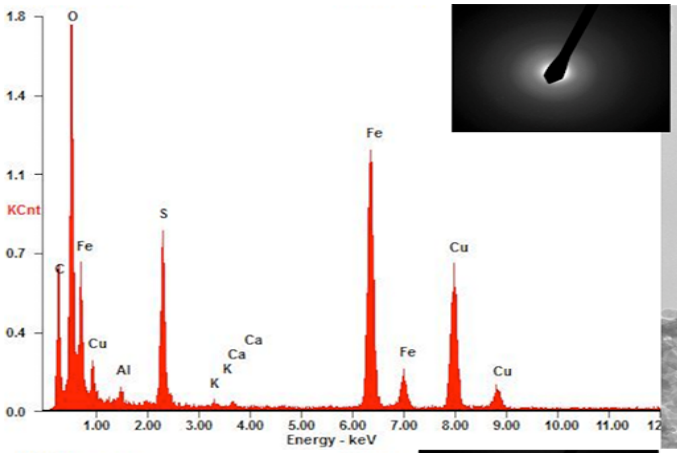
KCnt
Energy - keV
O
Fe
S
Cu
C
Al
K
Ca

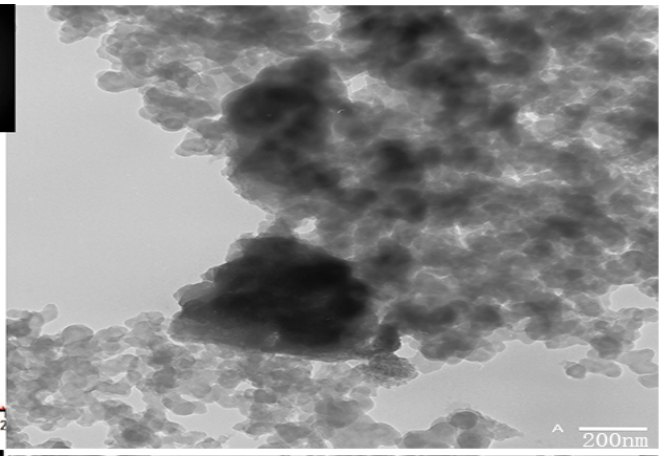
A
200nm

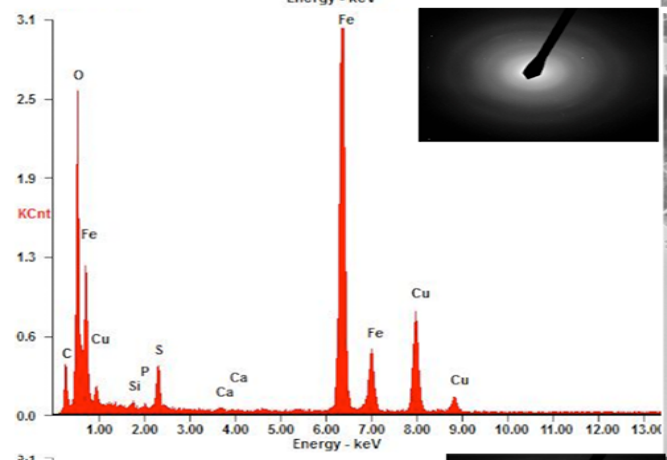
KCnt
Energy - keV
Fe
O
C
Cu
S
P
Si
Ca

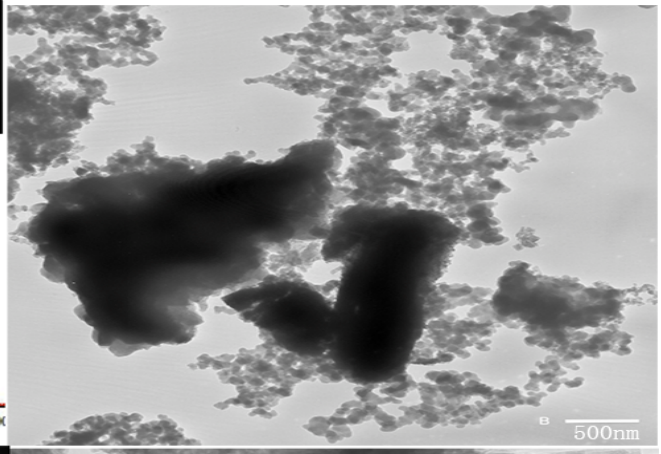
B
500nm

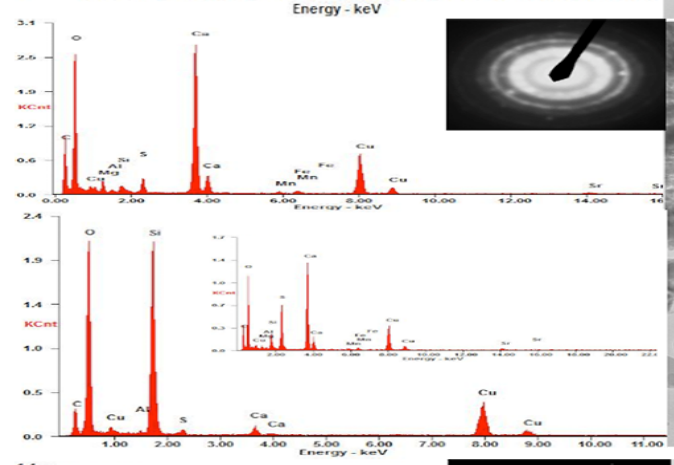
KCnt
Energy - keV
O
Si
Ca
Cu
Al
S
C

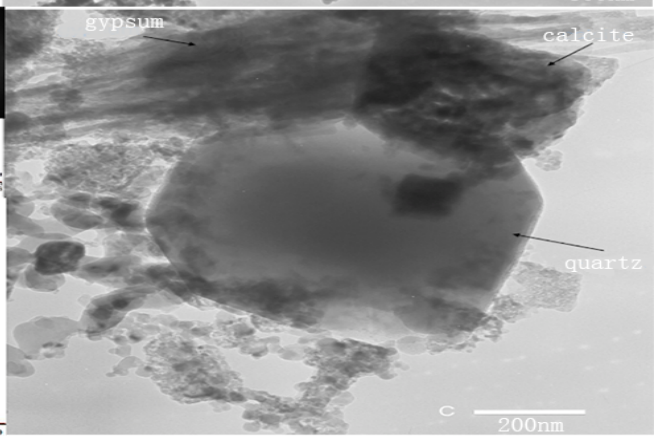
gypsum
calcite
quartz
C
200nm

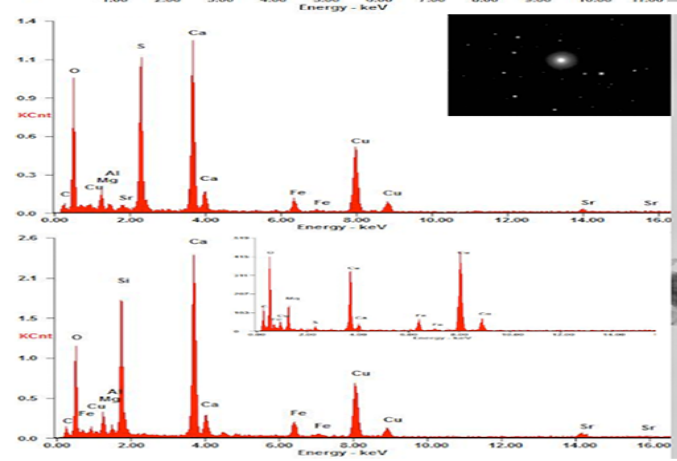
KCnt
Energy - keV
O
Ca
S
Si
Cu
Al
Mg
Fe
Sr

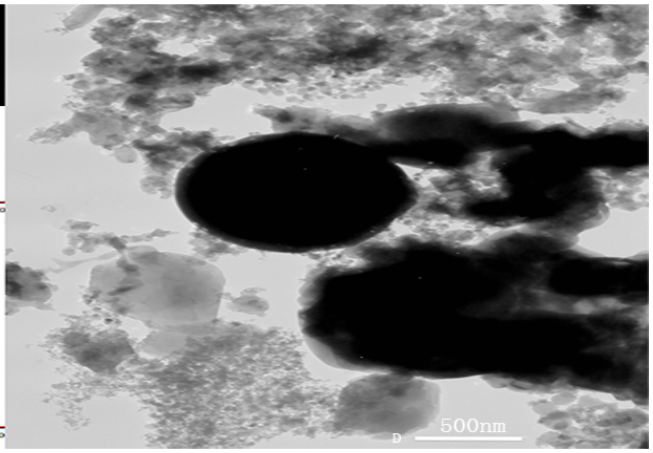
D
500nm

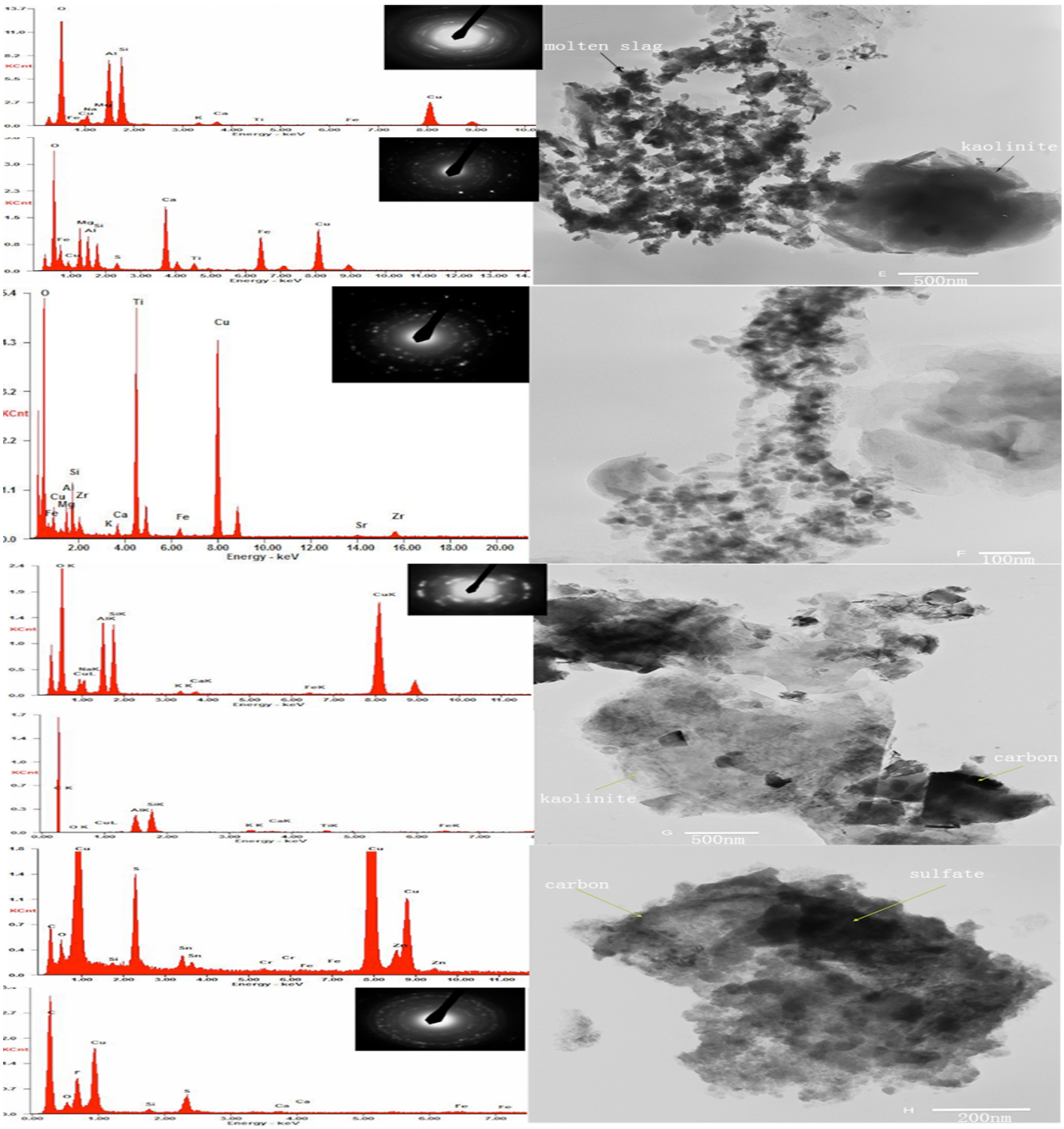

Figure S2 High-resolution microstructure of electron microscope images (right, white line is a standard index) and EDX spectra showing particle chemistry (left, in the inset electron diffraction pattern (EDP)) of solid sources: A. airborne organic substance with mineral particle in DTP (length 200 nm), the EDX and EDP shown as amorphous ferric sulfate ($Fe_2(SO_4)_3$); B. airborne organic substance with mineral particles in DTP (length 500 nm), shown as amorphous siderite; C. mineral particles in furnace fly ash (length 200 nm), shown as amorphous and crystalline phase particles (gypsum, calcite, quartz); D. airborne organic substance with mineral particles in furnace fly ash (length 500 nm), shown as silicate microbead; E. molten slags with clay mineral in stovepipe fly ash (length 500 nm), shown as the order mineral (kaolinite and illite); F. molten slags with authigenic minerals (length 100 nm), shown as rutile; G. carbon particle and clay minerals in honeycomb briquette (length 500 nm), shown as illite and kaolinite; and H. carbon particle and sulfate mineral particles (length 200 nm), shown enriched with metals (Cr-Fe-Zn-Sn-In).

Spectral analysis by curve fitting and parameters： Raman spectroscopy provides very reliable information on the degree of structural order, so this tool is widely used to distinguish a variety of chemical substances, including carbonaceous materials, soot and inorganic salts.[1] The shapes and intensities of the Raman bands of carbonaceous materials are functions of their crystal size, morphology and composition. The only peak of crystalline graphite (near 1580 cm^{-1}) is the G band, which is attributed to the stretching mode (E_2g symmetry) in the aromatic layers of the graphitic crystalline. The D1 band at 1350 cm^{-1} corresponds to a vibration mode (A_1g symmetry), which involves graphitic layer carbon atoms in the immediate vicinity of a lattice disturbance. The D2 band (~1620 cm^{-1}) and D3 band (~1500cm^{-1}) can be attributed to the E_2g symmetry of surface grapheme layers and amorphous carbon, such as organic molecules and functional groups, respectively. Additionally, the D4 band near 1200 cm^{-1} is associated with sp^2-sp^3 mixed states at the periphery of crystallites or C-C and C=C stretching vibrations of polygene-like structures (ionic impurities). Many reports provide explanations for these bands.[2] Recent studies have suggested that five bands in the observed spectra can be accounted by experimental observations and theoretical calculations.[3] By testing different band combinations of peak fitting, researchers found that the best combination for soot samples are four Lorentzian-shaped bands (G, D1, D2, D4) with a Gaussian-shaped band (D3).[4]

Many reports are about explanations of Raman spectroscopy parameters.

$$R1 = \frac{I_{D1}}{I_{D1} + I_{D2} + I_G} \qquad (1)$$

where I_{D1}, I_{D2}, I_G represent the intensity of D1, D2 and G band. R1 can characterize the order of carbonaceous matter.[5] All R1 parameters of the $PM_{2.5}$ samples are higher than 0.5, indicating that they are poorly organized. Furthermore, R1 parameters are all between 0.6 and 0.8 and have high consistency with time and space, so that it can be used to access the possible sources.

$$R2 = \frac{I_{D3}}{I_{D2} + I_{D3} + I_G} \qquad (2)$$

where I_{D2}, I_{D3}, I_G represent the intensity of D2, D3 and G band. R2 represents the amorphous carbon content, and the R2 value for most of the $PM_{2.5}$ and possible sources is between 0.1 and 0.3, while the minimum is 0.09 for the smoke of anthracite combustion and the maximum is 0.43 for gasoline vehicle exhaust. The relatively high R2 value of sample No. 3 indicates its close relationship with the gasoline vehicles, which is expected because this sample was collected near a busy road.

In most samples, the D1 band intensity is much higher than that of the other four bands. From crystallography views, it can be explained by the small crystal sizes. $PM_{2.5}$ samples each have a value between 200 cm^{-1} and 300 cm^{-1} for the D1 band FHWM. However, the FHWM values of D1 band for fly ashes from both the honeycomb and furnace are less than 100 cm^{-1}. According to the conclusions of a previous study,[6] compared to the high degree of structural order of coal and fly ashes, the structural order of $PM_{2.5}$ is relatively low and the chemical heterogeneity quite high partly due to the complexity of its sources and unclear changing process in the air.

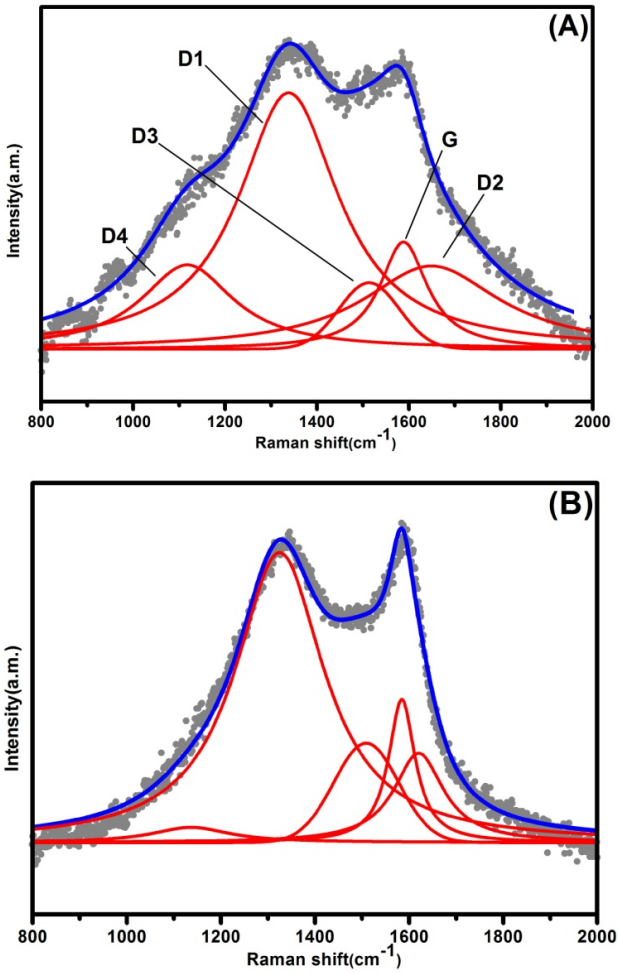

Figure S3 Raman spectrum of (A) $PM_{2.5}$ and (B) fly ash sample fitted using four Lorentzian and one Gaussian curves located at the frequencies of the G, D1 and D4 bands: thin solid curves (5), four Lorentzian and one Gaussian; solid curve (noisy), measured spectrum; and dashed curve, sum of Lorentzian and Gaussian curves.

Table S1 Spectral parameters for the first-order Raman bands of different $PM_{2.5}$, solid samples and emission sources (λ_0 = 633 nm), band position (Stokes Raman Shift, cm^{-1}), full width at half maximum (FWHM, cm^{-1}), and integrated band intensity ratios (Ix/Iy, arithmetic mean values).

Sample No. [a]		1	2	3	4	5	6	7	8	9
G	Position	1589	1590	1586	1580	1565	1583	1594	1591	1574
	FWHM	82	131	84	76	112	83	84	73	65
D1	Position	1360	1342	1330	1342	1350	1361	1353	1350	1337
	FWHM	228	237	242	292	262	249	277	297	402
	I_{D1}/I_G	4.34	2.13	4.93	4.64	3.78	4.78	5.78	6.88	13.20
D2	Position	1616	1634	1651	1617	1600	1619	1628	1636	1608
	FWHM	296	392	15	53	55	325	117	288	46
	I_{D2}/I_G	1.66	0.38	0.04	0.26	0.27	1.85	0.51	2.48	0.65
D3	Position	1513	1496	1510	1510	1506	1510	1525	1516	1511
	FWHM	82	123	132	76	81	83	110	117	85
	I_{D3}/I_G	0.43	0.23	0.44	0.33	0.15	0.35	0.77	0.76	0.59
D4	Position	1246	1131	1130	1122	1119	1241	1124	1120	1124
	FWHM	189	50	382	27	61	116	35	0	77
$R1=I_{D1}/(I_{G+} I_{D1+} I_{D2})$		0.62	0.61	0.82	0.79	0.79	0.75	0.63	0.66	0.89
$R2=I_{D3}/(I_{G+} I_{D2+} I_{D3})$		0.14	0.14	0.44	0.21	0.34	0.11	0.11	0.18	0.26

Sample No.		10	11	12	13	14	15	16	17	18	19
G	Position	1579	1594	1598	1615	1584	1597	1592	1582	1585	1562
	FWHM	49	95	71	64	68	93	81	102	88	106
D1	Position	1322	1352	1363	1397	1325	1370	1350	1348	1346	1349
	FWHM	91	206	323	74	230	263	296	250	319	240
	I_{D1}/I_G	5.29	2.08	9.66	0.90	6.21	4.12	4.28	2.30	6.07	4.18
D2	Position	1600	1625	1697	1696	1620	1596	1621	1622	1622	1612
	FWHM	30	29	345	122	128	249	183	108	64	92
	I_{D2}/I_G	0.71	0.10	5.35	1.72	1.12	1.13	0.31	0.06	0.28	1.30
D3	Position	1520	1510	1522	1521	1509	1525	1518	1503	1512	1504
	FWHM	193	150	63	147	162	111	110	76	166	133
	I_{D3}/I_G	0.96	0.51	0.78	1.66	1.16	0.58	0.65	0.10	0.97	0.80
D4	Position	1206	1230	1127	1331	1136	1124	1198	1202	1232	1212
	FWHM	393	328	20	264	203	22	88	102	60	106
$R1=I_{D1}/(I_{G+}I_{D1+}I_{D2})$		0.76	0.65	0.60	0.25	0.74	0.66	0.76	0.68	0.83	0.64
$R2=I_{D3}/(I_{G+}I_{D2+}I_{D3})$		0.36	0.32	0.11	0.38	0.35	0.21	0.33	0.09	0.43	0.26

References:

1 A. C. Ferraii and J. Robertson, Phys. Rev. B: Condens. Matter Mater. Phys., 2001, 64(075414), 1–13.

2 S.-K. Sze, N. Siddique, J. J. Sloan and R. Escribano, Atmos. Environ., 2001, 35, 561–568.

3 A. Sadezky, H. Muckenhuber, H. Grothe, R. Niessner and U. Poschl, Carbon, 2005, 43, 1731–1742.

4 N. P. Ivleva, A. Messerer, X. Yang, R. Niessner and U. Posghl, Environ. Sci. Technol., 2007, 41, 3702–3707.

5 O. Beyssac, B. Goffe, J. P. Petitet, E. Froigenux, M. Moreau and J. N. Rouzaud, Spectrochim. Acta, Part A, 2003, 59, 2267–2276.

6 Q. Yao, S. Li, H. Xu, J. Zhuo and Q. Song, Energy, 2009, 34, 1296–1309.